JOURNAL OF MOLECULAR SPECTROSCOPY 173, 452–462 (1995)

D_2 $E, F\ ^1\Sigma_g^+$ ($v' = 0$ and 1)–$X\ ^1\Sigma_g^+$ ($v'' = 0$–5) Transition Energies for $J' = J'' = 0$–26: Comparison of Experiment and Theory

ALBERT J. R. HECK,*† WINIFRED M. HUO,‡ RICHARD N. ZARE,† AND DAVID W. CHANDLER*

*Combustion Research Facility, Sandia National Laboratories, Livermore, California 94551; †Department of Chemistry, Stanford University, Stanford, California 94305; and ‡NASA Ames Research Center, Moffett Field, California 94035

Received February 27, 1995

The bimolecular gas-phase reaction between suprathermal atomic deuterium atoms and jet-cooled deuterium iodide, D + DI → D_2 + I, was used to generate a wide range of rovibrationally excited deuterium molecules, D_2. Using (2 + 1) resonance-enhanced multiphoton ionization spectroscopy, we measured many previously unreported $E, F\ ^1\Sigma_g^+$ ($v'_E = 0$ and 1, $J' = J''$)–$X\ ^1\Sigma_g^+$ ($v'' = 0$–5, J'') two-photon transition energies, for rotational levels that range from $J'' = 0$ to 26. Experimental observation of many transitions corresponding to high rotational levels allowed the testing of higher-order molecular constants for the $X\ ^1\Sigma_g^+$ ground state as well as for the $E, F\ ^1\Sigma_g^+$ excited electronic state. Significant discrepancies were found between observed transition energies and those calculated from known molecular constants (i.e., more than a few hundred cm^{-1}) for the higher rotational levels. Separately, rovibrational term values of the $X\ ^1\Sigma_g^+$ ground state and $E, F\ ^1\Sigma_g^+$ state were calculated, using *ab initio* methods, to provide calculated transition energies. Excellent agreement is observed between the experimental and *ab initio* calculated transition energies, which confirms the accuracy of the theoretical potentials.

INTRODUCTION

Characterization of the energy levels of molecular hydrogen and its isotopomers is a classic problem in molecular spectroscopy. The ground state of molecular deuterium, the molecule of interest in this study, has been characterized in such detail that little would seem to remain unknown about its nature and energy levels. Although this assumption is true for low rotational levels over a wide range of vibrational states, whose energies are accurately known to within hundredths of cm^{-1} (*1*), it is not true for the higher rotational energy levels. Even for the $X\ ^1\Sigma_g^+$ ground state, only the relatively low rotational levels J'' have been identified experimentally (typically $J'' <$ 10 for $v'' = 0$–1) (*1–4*). As shown below, molecular constants derived from this limited set of data are not accurate enough to describe higher rotational energy levels.

The various electronic and rovibronic levels of molecular deuterium have been identified using absorption and emission spectroscopy (*3, 5–9*), spontaneous Raman scattering (*1*), coherent anti-Stokes Raman scattering (CARS) (*10*), and resonance-enhanced multiphoton ionization (REMPI) spectroscopy (*11–16*). Various electronic states of D_2 have been characterized, and tables of rovibronic term values have been compiled (*17*). So far, numerous electronic and corresponding vibrational states have been studied experimentally, but only a relatively small range of rotational states has been covered. Because of the large rotational constants of ground state molecular deuterium ($B_0 \approx 30\ cm^{-1}$), which result in widely spaced rotational energy levels,

0022-2852/95 $12.00

only a few of the lowest rotational levels are populated at room temperature. Exciting molecular deuterium by using a discharge source leads to relatively little rotational excitation, although high vibrational levels can be populated in this manner (*5*). Thus, acquiring high rotational excitation of molecular deuterium requires the use of alternative methods.

A carefully chosen photodissociation or bimolecular reaction can efficiently generate highly rotationally excited molecules (*10, 18, 19*). For example, the H + HI → H_2 + I reaction has been used to generate highly excited rovibrational levels of H_2, whose ground state X $^1\Sigma_g^+$ (v'', J'') energy levels were subsequently identified using CARS (*10*) and (2 + 1) REMPI spectroscopy via the E, F $^1\Sigma_g^+$ electronic state (*18*). The latter (2 + 1) REMPI detection scheme has been widely used for the determination of H_2 population distributions in combustion environments and for the study of gas-phase (*18, 20–28*) and surface reactions (*29*). For a somewhat limited set of rovibrational levels, this REMPI scheme has been used previously to detect D_2 as well (*16, 20*). This REMPI scheme enables ultrasensitive and state-selective detection of scattered reaction products and trace gasses (*27, 28, 30*). However, reliable use of this scheme requires accurate knowledge and precise assignments of the transition energies for a broad range of rotational and vibrational levels.

Theoretical calculations are not hampered by the above-mentioned experimental obstacles, and high-level *ab initio* calculations have been reported for the X $^1\Sigma_g^+$ ground state for a wider range of rotational levels than observed experimentally. Several high-level *ab initio* calculations show close agreement with experimentally established data for low rotational levels (*31–35*). In a recent study Yu and Dressler (*35*) calculated the rovibronic structures for all electronic states below the $1s + 2l$ dissociation limit, incorporating both adiabatic corrections and nonadiabatic coupling. Only rotational levels up to $J = 5$ were considered, however.

The lowest $^1\Sigma_g^+$ excited electronic state of molecular deuterium, the $^1\Sigma_g^+$ E, F state, is characterized by a double-minimum potential. Both the inner well (E state) and the outer well (F state) support bound vibrational levels. In the inner well, four vibrational levels are located, $v_E = 0$, 1, 2, and 3, respectively, which correspond with $v_{EF} = 0$, 2, 6, and 9. The ordering of the vibrational levels in the inner and outer wells is J-dependent, however, as the rotational energy spacing in the outer F well is smaller than in the inner well. Recently, accurate characterization of the E, F $^1\Sigma_g^+$ state has become an important parameter in the precise determination of the ionization potential of D_2 (*4, 14, 36*). Reported rovibrational levels of the E, F $^1\Sigma_g^+$ state of molecular deuterium identified via emission spectroscopy generally cover a wide range of vibrational levels (*3, 5*), but once more the observed range of rotational levels is limited from, typically, $J' = 0$ to 10. The currently used rotational constants (*37*) for the first two vibrational levels of the E state have been determined from this rather small range of rotational states. The E, F $^1\Sigma_g^+$ state of molecular deuterium has also been characterized theoretically (*35, 38–41*).

In the present study we measured rovibrational population distributions of D_2 formed via the D + DI → D_2 + I reaction for $v'' = 0$ to $v'' = 5$, observing rotational levels ranging from $J'' = 0$ to 26. D_2 was detected using (2 + 1) REMPI spectroscopy via the E, F $^1\Sigma_g^+$ state. The rovibrational distributions and velocity distributions of the D_2 products will be reported elsewhere (*30*). Here we compare experimentally determined E, F $^1\Sigma_g^+$ ($v'_E = 0$ and 1, $J' = J''$)–X $^1\Sigma_g^+$ ($v'' = 0$–5, J'') transition energies, measured in units of cm^{-1}, with our calculated values and with transition energies obtained from currently available molecular constants for the X $^1\Sigma_g^+$ ground state and the E, F $^1\Sigma_g^+$ excited state.

METHODOLOGY

Experimental Procedures

REMPI spectra of D_2 were recorded using an ion-imaging apparatus described previously (*42*). In brief, DI (Cambridge Isotopes Laboratories, 99% D, backing pressure 8 psig [150 kPa]) is expanded supersonically into a source vacuum chamber through a solenoid valve (General Valve Series 9). Approximately 1 cm from the nozzle surface, the beam is skimmed (Beam Dynamics, orifice, 0.8 mm diameter) and collimated by a hole (1 mm diameter) in the repeller plate. The background pressure in the detection chamber is typically 10^{-6} Pa and increases to 10^{-5} Pa when the pulsed (30 Hz) DI molecular beam is on. Translationally hot D atoms, formed in the beam via photolysis of DI, subsequently react with the residual DI in the beam to produce the D_2 (v, J) products; that is, the single beam expansion provides both reagents needed for the reaction. Under our experimental conditions, the collision energies for the D + DI reaction reach 3 eV. Additionally, the D + DI → D_2 + I reaction is exothermic by 1.46 eV. These conditions result in the formation of highly internally excited rovibrational product states of molecular deuterium.

In our experiments, a single ultraviolet laser pulse is used to photolyze the DI and to photoionize and detect the D_2 (v, J) products. Thus, photolysis, reaction, and state-selective product ionization occur during a single laser pulse ($\approx$5-nsec duration). The laser wavelengths in the (2 + 1) REMPI spectra range from 204 to 236 nm. Generation of the required UV laser pulses is done by frequency doubling (Inrad) of an injection-seeded Nd:YAG-pumped dye laser (Spectra Physics GCR5, PDL 2) using KD*P crystals. The frequency-doubled dye output is sum-frequency mixed (Inrad) with the residual dye laser fundamental using appropriate BBO crystals. For the 204- to 233-nm wavelength range we use several dyes (R640, a mixture of R640 and DCM, DCM, and LDS 698). UV output powers are kept constant as much as possible at 300 ± 30 μJ per pulse. The bandwidth of the UV laser pulses is less than 1 cm^{-1}. Using dichroic mirrors, we cross the UV light with the molecular beam and focus it using a lens (f = 15 cm). After the state-selective photoionization of D_2 (v, J) molecules, D_2^+ ions are accelerated along a 20-cm-long flight tube and impinge on a two-dimensional, position-sensitive detector. The detector consists of a pair of chevron microchannel plates (Galileo, 7.62 cm diameter) coupled to a fast phosphor screen (P47 Phosphor, 80-nsec decay time). Mass-selective detection of the D_2^+ ions is accomplished by setting a boxcar gate on the D_2^+ mass peak in the time-of-flight spectrum. The integrated phosphorescence of the phosphor screen, induced by impinging ions on the microchannel plates, is recorded using a photomultiplier tube.

Ab Initio Calculations

Theoretical transition energies are obtained from the differences between the *ab initio* rovibrational energies of the $X\,^1\Sigma_g^+$ and $E, F\,^1\Sigma_g^+$ states of D_2 plus the differences between their electronic term values (*37*). The rovibrational energy levels of each electronic state are obtained by solving the rovibrational Schrödinger equation for each pair of (v, J) energy levels. For the $X\,^1\Sigma_g^+$ state, the adiabatic potential tabulated by Schwartz and Le Roy (*33*), which includes both relativistic and radiative corrections, was used for the vibrational motion, and for the $E, F\,^1\Sigma_g^+$ state, the nonrelativistic adiabatic potential came from the work of Wolniewicz and Dressler (*43*). The Numerov–Cooley (see Refs. *44*, *45*) method was employed for the numerical solution of the one-dimensional Schrödinger equation of vibrational motion.

Note that analytical expressions for the nonadiabatic energy corrections of the rovibrational levels of the $X\ ^1\Sigma_g^+$ are available (*33, 46*). However, in view of the fact that the corresponding analytical corrections are not available for the E, $F\ ^1\Sigma_g^+$ state (*35, 47*), the present calculations employ the adiabatic approximation throughout, so that the transition energies are determined at a given level of approximation. Comparing our calculated adiabatic dissociation energies of the ground state with Wolniewicz's nonadiabatic results (*46*) available for $v = 0$–5 and $J \leq 10$, it is found that the nonadiabatic correction is dependent on J and v. For $J = 0$, the nonadiabatic correction is 0.02 cm^{-1} at $v = 0$ and increases to 0.27 cm^{-1} at $v = 5$. For $J = 10$ the v-dependence is much weaker; the nonadiabatic correction varies from 0.68 cm^{-1} at $v = 0$ to 0.81 cm^{-1} at $v = 5$. Comparing the adiabatic energies of the E state with the nonadiabatic results of Yu and Dressler (*35*) available for $J \leq 5$ shows that at $J = 0$ the difference is 1.34 and 1.88 cm^{-1} for $v = 0$ and 1, respectively. At $J = 5$, the difference is 1.22 and 2.06 cm^{-1}. Thus the nonadiabatic corrections for the E state are larger than those for the X state. It is expected that the nonadiabatic corrections for the E state levels will be larger at high J.

RESULTS AND DISCUSSION

More than 200 resonant transitions have been observed in the wavelength range studied. Part of the D_2 REMPI spectrum is shown in Fig. 1, together with some of the assignments. Only Q-branch transitions are observed. While O- and S-branch

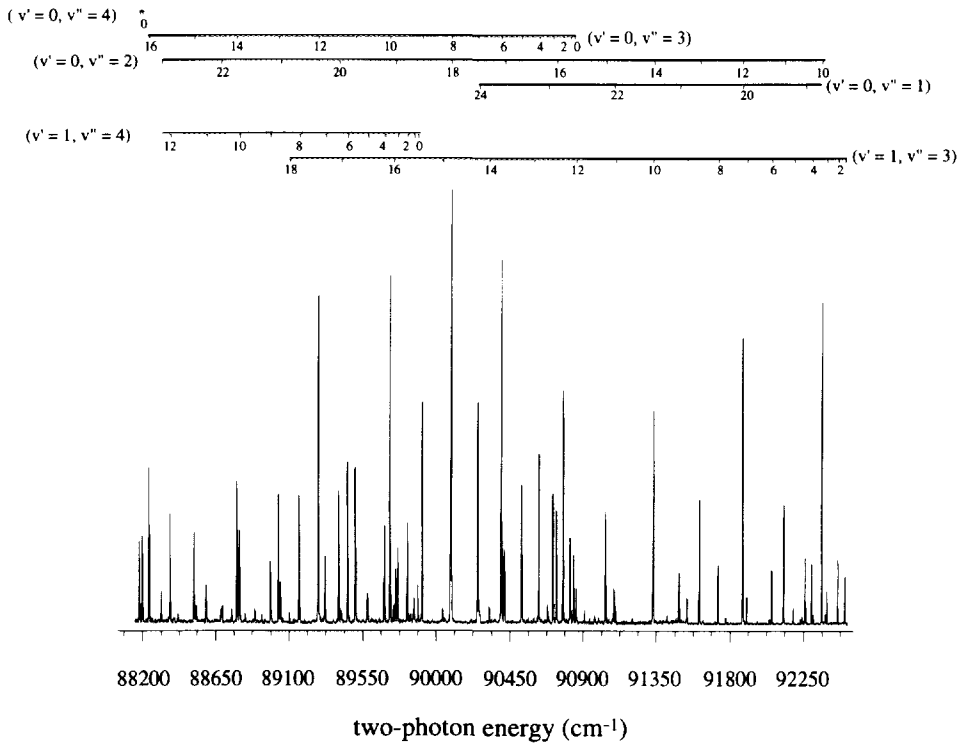

FIG. 1. (2 + 1) REMPI spectrum of the D_2 E, $F\ ^1\Sigma_g^+$ ($v'_E = 0$ and 1, $J' = J''$)–$X\ ^1\Sigma_g^+$ ($v'' = 1$–4, J'') bands between 88 200 and 92 300 cm^{-1}. The assigned Q-branch transitions are indicated at the top of the figure.

TABLE I

Calculated versus Observed $E, F\ ^1\Sigma_g^+\ v_{E'} = 0, J' = J'')$–$X\ ^1\Sigma_g^+\ (v_{X''}, J'')$ Transition Energies (cm^{-1})

J"=J	v"=0 [a]	v"=0 [b]	v"=1 [a]	v"=1 [b]	v"=2 [a]	v"=2 [b]	v"=3 [a]	v"=3 [b]	v"=4 [a]	v"=4 [b]	v=5 [a]	v"=5 [b]
0		99460.11	96469	96466.56	93592	93592.10	90835	90834.67	88194	88192.60	85666	85664.71
1		99432.38	96441	96440.94	93570	93568.56	90813	90813.16	88174	88173.11	85647	85647.24
2		99377.07	96391	96389.83	93523	93521.59	90771	90770.28	88139	88134.26	85614	85612.39
3		99294.45	96310	96313.52	93454	93451.47	90706	90706.26	88081	88076.28	85559	85560.41
4		99184.95	96213	96212.39	93363	93358.57	90622	90621.47	88003	87999.52	85492	85491.61
5		99049.10	96086	96086.96	93243	93243.38	90516	90516.37	87906	87904.41	85407	85406.43
6		98887.58	95940	95937.87	93109	93106.51	90392	90391.55	87794	87791.51	85306	85305.38
7		98701.14	95764	95765.83	92947	92948.64	90248	90247.65	87662	87661.44	85188	85189.05
8		98490.65	95573	95571.69	92771	92770.56	90083	90085.42	87515	87514.91	85059	85058.13
9		98257.06	95353	95356.32	92571	92573.12	89903	89905.67	87350	87352.68	84914	84913.33
10		98001.35	95119	95120.67	92353	92357.20	89709	89709.24	87175	87175.56		84755.41
11	97726	97724.60	94867	94865.76	92123	92123.78	89500	89497.04	86982	86984.40		84585.20
12	97428	97427.90	94593	94592.62	91876	91873.83	89272	89270.00	86778	86780.09		84403.53
13	97113	97112.36	94297	94302.29	91613	91608.33	89027	89029.05	86562	86563.51		84211.23
14	96780	96779.11	93990	93995.85	91331	91328.31	88776	88775.16	86331	86335.57		84009.18
15	96430	96429.29	93675	93674.37	91036	91034.76	88508	88509.27	86096	86097.16		83798.21
16	96071	96064.01	93336	93338.89	90733	90728.68	88231	88232.30	85847	85849.17		83579.17
17	95692	95684.37	92988	92990.45	90415	90411.04	87945	87945.20	85592	85592.46		83352.88
18	95289	95291.43	92637	92630.04	90087	90082.77	87650	87648.82	85325	85327.87		83120.14
19	94890	94886.25	92263	92258.65	89748	89744.81	87340	87344.07	85059	85056.25		82881.77
20	94464	94469.70	91879	91877.12	89403	89397.93	87030	87031.65		84778.25		82638.41
21	94035	94043.03	91489	91486.60	89046	89043.26	86709	86712.65		84494.94		82391.08
22	93609	93606.25	91083	91087.08	88684	88680.70	86386	86386.94		84206.16		82139.61
23	93162	93161.66	90677	90680.80	88312	88312.46	86055	86056.69		83914.04		81886.15
24	92705	92704.86	90257	90263.30	87938	87934.06	85715	85717.37		83614.06		81626.17
25	92246	92245.48	89845	89844.18	87559	87555.05	85382	85378.52		83315.73		81369.21
26	91776	91781.28		89421.15	87174	87173.11	85035	85037.82		83016.74		81113.00
27		91276.13		88958.06		86752.06		84659.05		82680.91		80821.44
28		90809.57		88534.42		86371.42		84321.74		82387.77		80574.15
29		90337.70		88106.30		85987.22		83981.95		82093.46		80327.34
30		89886.44		87699.63		85625.40		83665.63		81823.98		80107.09

a. Experimentally obtained transition energies.
b. Calculated transition energies.

transitions are also allowed by symmetry, they are known to be very weak (*14*). In Tables I and II, the two-photon transition energies (in cm^{-1}) of the observed $E, F\ ^1\Sigma_g^+\ (v'_E = 0, J' = J'')$–$X\ ^1\Sigma_g^+\ (v'' = 0\text{–}5, J'')$ and $E, F\ ^1\Sigma_g^+\ (v'_E = 1, J' = J'')$–$X\ ^1\Sigma_g^+\ (v'' = 1\text{–}5, J'')$ transitions are given, respectively. Because of the high center-of-mass collision energy and high exothermicity of the reaction used to generate the deuterium molecules, the D_2 products are formed with a broad range of translational energies (*30*). Therefore, the Doppler bandwidths of many of the observed transitions are close to 10 cm^{-1}, much broader than the laser bandwidth. Partly because of these

TABLE II

Calculated versus Observed $E, F\ ^1\Sigma_g^+\ (v_{E'} = 1, J' = J'')$–$X\ ^1\Sigma_g^+\ (v_{X''}, J'')$ Transition Energies (cm^{-1})

J"=J	v"=0 [b]	v"=1 [a]	v"=1 [b]	v"=2 [a]	v"=2 [b]	v"=3 [a]	v"=3 [b]	v"=4 [a]	v"=4 [b]	v"=5 [a]	v"=5 [b]
0	101149.01		98155.45	95283	95281.00	92524	92523.56	89882	89881.49	87354	87353.61
1	101119.92		98128.47	95256	95256.09	92503	92500.70	89862	89860.65	87335	87334.77
2	101061.89		98074.65	95208	95206.41	92456	92455.10	89821	89819.08	87297	87297.21
3	100975.21		97994.28		95132.23	92392	92387.02	89761	89757.04	87244	87241.17
4	100860.29		97887.73	95034	95033.91	92296	92296.81	89677	89674.86	87165	87166.96
5	100717.69	97756	97755.55	94910	94911.97	92187	92184.96	89573	89573.00	87076	87075.02
6	100548.14	97600	97598.43	94767	94767.06	92052	92052.11	89456	89452.07	86966	86965.94
7	100352.23	97418	97416.93	94603	94599.73	91901	91898.74	89316	89312.54	86842	86840.15
8	100131.01	97213	97212.05	94413	94410.92	91728	91725.78	89157	89155.27	86697	86698.49
9	99885.367	96985	96984.63	94202	94201.43	91533	91533.98	88982	88980.99	86544	86541.64
10	99616.313	96739	96735.63	93973	93972.16	91324	91324.19	88794	88790.51	86367	86370.37
11	99324.930	96471	96466.09	93728	93724.11	91098	91097.37	88587	88584.73	86184	86185.53
12	99012.203	96180	96176.92	93461	93458.13	90854	90854.30	88365	88364.40	85986	85987.83
13	98679.281	95870	95869.21	93178	93175.26	90597	90595.98	88128	88130.44	85777	85778.16
14	98327.523	95545	95544.26	92879	92876.72	90324	90323.57	87880	87883.98	85557	85557.58
15	97957.352	95208	95202.43		92562.82	90043	90037.33	87623	87625.22	85326	85326.27
16	97568.250	94847	94843.13	92226	92232.93	89736	89736.55	87346	87353.41	85084	85083.41
17	97167.477	94477	94473.55		91894.14	89425	89428.30	87073	87075.57		84835.98
18	96746.102	94088	94084.71		91537.44	89100	89103.49	86784	86782.55		84574.82
19	96318.039	93691	93690.45		91176.61		88775.86	86484	86488.04		84313.57
20	95861.531	93273	93268.94		90789.76		88423.48	86167	86170.08		84030.24
21	95417.273	92847	92860.84		90417.50		88086.89		85869.12		83765.32
22	94868.547		92349.38		89943.00		87649.24		85468.46		83401.91
23	94437.211		91956.35		89588.02		87332.24		85189.59		83161.70

a. Experimentally obtained transition energies.
b. Calculated transition energies.

broad bandwidths, some transition energies are observed to overlap. The wavelength of the UV laser was calibrated at a single frequency that corresponds to the (2 + 1) Lyman β resonance of the D atom. The uncertainties in some of the experimental transition energies are therefore rather large, approximately 2 cm^{-1}. The ion images reveal that some of the D_2 is not formed in the bimolecular reaction, D + DI → D_2 + I, but via unimolecular photoinduced chemistry involving DI dimers or higher clusters. The role of cluster chemistry will be addressed in a future report (*30*), but has no consequences for the spectroscopy of the D_2 molecule, as presented here. In Tables I and II, the experimentally observed transition energies are given.

In Figs. 2A and 2B the observed transition energies are compared with transition energies obtained using available molecular constants. We used the Dunham notation in which the term values may be expressed by (*37*)

$$T_{v,J} = T_e + \Sigma_{ij}\, Y_{ij}\,(v + \tfrac{1}{2})^i\, J^j\,(J + 1)^j. \qquad (1)$$

The observed Q-branch transition energies ($J' = J''$) correspond to

$$\Delta E = (T_e' - T_e'') + \Sigma_{i'j'}\, Y_{i'j'}(v' + \tfrac{1}{2})^{i'}\, J^{j'}\,(J + 1)^{j'} - \Sigma_{i''j''}\, Y_{i''j''}(v'' + \tfrac{1}{2})^{i''}\, J^{j''}\,(J + 1)^{j''}. \qquad (2)$$

Figures 2A (for $v_{E'} = 0$) and 2B (for $v_E' = 1$) show the differences, in cm^{-1}, between the observed transition energies and those obtained using parameters from Bredohl and Herzberg for the $X\ ^1\Sigma_g^+$ ($v'' = 0$–5, J'') ground state (*3*) and parameters from Huber and Herzberg (*37*) for the $E\ ^1\Sigma_g^+$ ($v_E' = 0$ and 1, J') excited state. Good agreement is observed between the experimental data and the data obtained from available spectroscopic constants for low rotational levels. Increasingly poor agreement is found, however, for higher rotational levels, which leads to deviations of more than several hundred cm^{-1} for $J > 20$ (Figs. 2A and 2B). At these high rotational levels, the experimentally observed transition energies are significantly lower than those obtained using the above-mentioned molecular constants.

Also in Tables I and II, the transition energies are given obtained from our *ab initio* calculations. In Figs. 3A (for $v_E' = 0$) and 3B (for $v_E' = 1$), the differences are shown between the observed and the *ab initio* transition energies; very good agreement is found. In general the differences fall within a few cm^{-1}. For higher J levels, slightly larger deviations seem to arise. These nonsystematic deviations may be caused partly by the weak intensities of these lines in the experimental spectra and the resulting difficulties in assigning them accurately. On the other hand, our calculations did not take nonadiabatic coupling or relativistic effects into account for the E, $F\ ^1\Sigma_g^+$ state. Relativistic effects are expected to be very small. Nonadiabatic coupling, however, can be large, especially for the high J' levels of the E, $F\ ^1\Sigma_g^+$ state, because of interactions with other nearby excited states (*35*). Therefore, some of the discrepancies between the observed and calculated transition energies may be genuine, because the measurements reveal the true E, $F\ ^1\Sigma_g^+$–$X\ ^1\Sigma_g^+$ transitions, whereas the calculations are based on adiabatic energy levels.

The data presented in Fig. 2 clearly show the inadequacy of published molecular constants in describing the observed transition energies for high J. As mentioned above, rotational molecular constants for the $X\ ^1\Sigma_g^+$ and the E, $F\ ^1\Sigma_g^+$ state have been determined from low rotational levels. These constants are probably accurate for B_v and to some extent for D_v, but they are not very accurate for H_v, which becomes an increasingly important parameter for the higher rotational levels. The data presented in Figs. 2A and

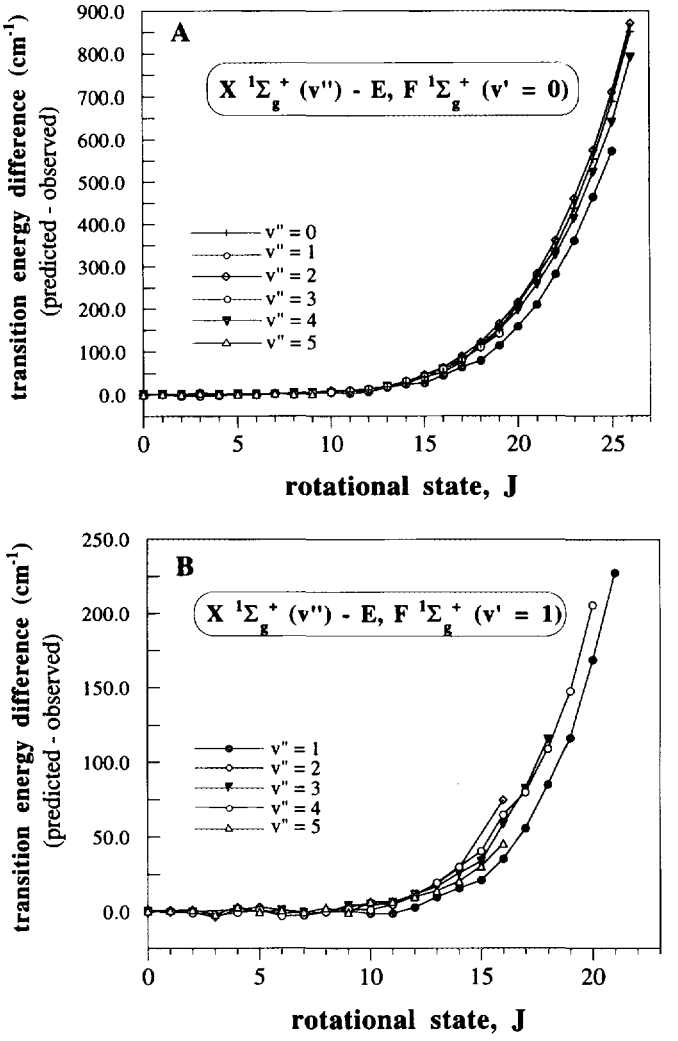

FIG. 2. (A) Energy differences (cm^{-1}) between the experimentally observed transition energies and those predicted by using molecular constants from Bredohl and Herzberg for the $X\ ^1\Sigma_g^+$ ($v'' = 0$–4, J'') ground state (*3*) and parameters from Huber and Herzberg (*37*) for the $E\ ^1\Sigma_g^+$ ($v_E' = 0$, J') excited state. (B) As in Fig. 2A for transitions to the $E\ ^1\Sigma_g^+$ ($v_E' = 1$, J') excited state.

2B reveal indirect information on the accuracy of the molecular constants used for the $X\ ^1\Sigma_g^+$ ground state. The depicted transition energy differences corresponding to the various ground state vibrational levels, v'', should overlay exactly if the ground state parameters used were "perfectly" correct. The data shown in Fig. 2A reveal that the $v'' = 1$ data in particular deviate significantly from the other v'' data. This divergence is confirmed by the data presented in Fig. 2B. Interestingly, $D_{v''=1}$ derived from experimental results by Bredohl and Herzberg (*3*) was shown to be too low to fit on a continuous plot of $D_{v''}$ versus v''. Our experimental data support a relative upward correction for $D_{v''=1}$, which would bring the data in Figs. 2A and 2B in better agreement with each other.

Description of the energy levels of the E well of the $E, F\ ^1\Sigma_g^+$ state by means of

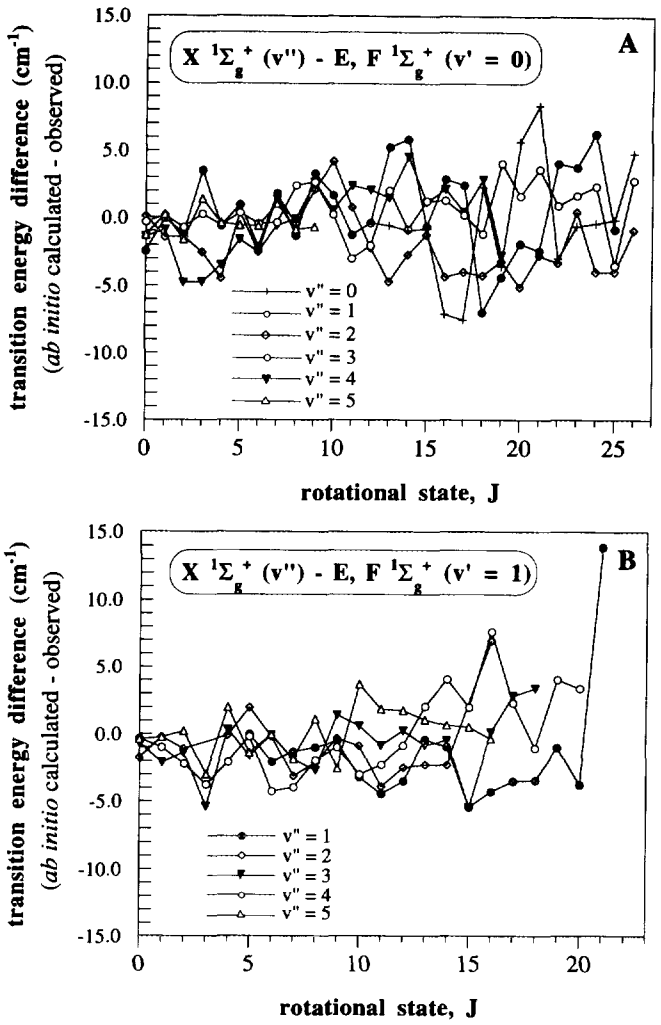

FIG. 3. (A) Energy differences (cm^{-1}) between the experimentally observed and the *ab initio* calculated transition energies to the $E\ ^1\Sigma_g^+$ ($v'_E = 0$) excited state. (B) As in Fig. 3A for transitions to the $E\ ^1\Sigma_g^+$ ($v'_E = 1$) excited state.

molecular constants is valid only for low J values, because the higher J levels are perturbed by levels located in the outer F well. Below the barrier between the E and F wells, perturbations of levels in the inner E well by the levels in the outer F well depend strongly on the energy difference between the two levels: the nearer the two levels are to each other in energy, the stronger the perturbation. These perturbations can dramatically affect the Franck–Condon factors and the two-photon transition moments as F-character becomes added to the wavefunction (*25, 40*). Only moderate change is expected, however, for the E well rovibrational energies. Close to or above the barrier between the two wells of the $E, F\ ^1\Sigma_g^+$ state, the rovibrational energy levels can no longer be described by the rotational constants used to describe a single "isolated" well. To illustrate these effects, rotational constants for the E well of the $E, F\ ^1\Sigma_g^+$ state were derived from the calculated rovibrational energies for $v' = 0$ and $v' =$

1, including in the fit only rovibrational energies of J' levels "reasonably" far below the barrier. For $v' = 0$, the lowest 27 levels were used ($J' = 0$–26) and for $v' = 1$ the lowest 19 rotational levels were used. Figure 4 depicts the energy differences between the rovibrational energies calculated by directly solving the rovibrational Schrödinger equation and those energies obtained using the molecular constants derived from the lower range of J' levels. Clearly, the derived molecular constants describe the rotational energy levels of the E well quite accurately up to $J' = 23$ for $v' = 0$ and up to $J' = 15$ for $v' = 1$. As shown, the deviations become dramatic and nonsystematic for higher J' levels, which indicates that the single-well description used in the fit is no longer appropriate for these J' levels. Our limited experimental data on the higher J' levels confirm the calculated effects. Unfortunately, no transition energies were observed for J' levels above 26 for $v' = 0$ and above 21 for $v' = 1$; such observations would have allowed us to test these theoretical findings in more detail.

In addition, the observed ion intensities (not shown) (*30*) allow us to compare the relative two-photon transition moments for the $E, F\,^1\Sigma_g^+ (v'_E = 0, J' = J'')$–$X\,^1\Sigma_g^+ (v'', J'')$ and $E, F\,^1\Sigma_g^+ (v'_E = 1, J' = J'')$–$X\,^1\Sigma_g^+ (v'', J'')$ transitions. Because of the multiphoton nature of the detection scheme, intensities obtained from the observed ion signal are not straightforward. To obtain signal intensities, the laser power was kept constant as much as possible. Spectra were then normalized for laser power dependence using previously obtained correction factors; that is, the ion signals were found to be proportional to the laser pulse energy raised to a power of 1.4 (*16*). Table III lists the experimentally observed and calculated relative intensity ratios. Again, the agreement between the experimental and theoretical data is very good. In general, the transitions via the $E, F\,^1\Sigma_g^+ (v'_E = 0)$ intermediate level are much stronger than those via the $E, F\,^1\Sigma_g^+ (v'_E = 1)$ intermediate level for $v'' = 1$, 2, and 3 vibrational levels of the $X\,^1\Sigma_g^+$ ground state. For $v'' = 4$ and 5, however, the scheme using the $E, F\,^1\Sigma_g^+ (v'_E = 1)$ intermediate level is the more sensitive choice for detection by (2 + 1) REMPI spectroscopy.

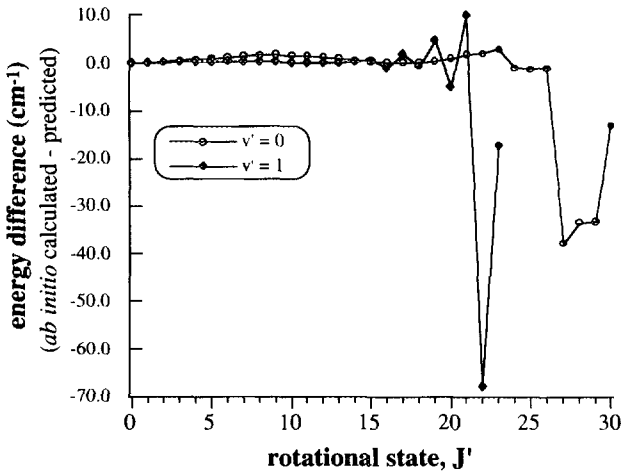

FIG. 4. Energy differences (cm^{-1}) between rovibrational energies of the $E\,^1\Sigma_g^+ (v'_E = 0$ and 1) state obtained by directly solving the rovibrational Schrödinger equation and those energies calculated using molecular constants obtained from a limited set of rovibrational energies (corresponding to lower J' values). See text for further explanation.

TABLE III

Calculated and Measured Relative Intensity Ratios in D_2 (2 + 1) E, $F\ ^1\Sigma_g^+$ (v' = 0 and 1)–$X\ ^1\Sigma_g^+$ (v'' = 1–5) REMPI Detection[a]

v"	Intensity ratio calculated E, v' = 0 : E, v' = 1	Intensity ratio experimental E, v' = 0 : E, v' = 1
1	1.3 : 1	1.52 : 1
2	6.2 : 1	9.2 : 1
3	8.1 : 1	11 : 1
4	0.7 : 1	1 : 1
5	1 : 4.8	1 : 4.2

[a] Calculations were carried out for J = 8 only; experimental values are averaged over a range of rotational levels J, typically J = 5 to 10. Errors in the experimental ratios are up to 25%.

CONCLUSIONS

Using a gas-phase bimolecular reaction, D + DI → D_2 + I, a wide range of rovibrational levels of D_2 can be populated. This approach has allowed us, using (2 + 1) resonance-enhanced multiphoton ionization spectroscopy, to observe new E, $F\ ^1\Sigma_g^+$ (v'_E = 0 and 1, J' = J'')–$X\ ^1\Sigma_g^+$ (v'' = 0–5, J'') two-photon transition energies for rotational levels that range from J'' = 0 to 26. Our experimental data are used to examine reported values for molecular constants for the $X\ ^1\Sigma_g^+$ ground state as well as the E, $F\ ^1\Sigma_g^+$ state. Poor agreement is found for high rotational levels. Rovibronic term values of the $X\ ^1\Sigma_g^+$ ground state and E, $F\ ^1\Sigma_g^+$ state were calculated, using *ab initio* methods, providing calculated two-photon transition energies. Excellent agreement is found between the observed and *ab initio* transition energies. Therefore, the adiabatic potentials tabulated by Schwartz and Le Roy (*33*) for the $X\ ^1\Sigma_g^+$ state and by Wolniewicz and Dressler (*43*) for the E, $F\ ^1\Sigma_g^+$ state describe the rotational energy levels, at least for relatively low vibrational levels, extremely well, even for very high J values. Experimental and theoretical results reveal the influence of the F outer well on the energy levels of the inner E well. Reasonably far below the barrier between the E and F wells, perturbations by the F well levels do not lead to significant energy shifts of the E well levels. At rotational levels close to or above the barrier, the effects induced by the presence of the outer F well are quite dramatic, and the rovibrational energy levels can no longer be described by a single potential well.

Measured and calculated signal intensities reveal that when applying the (2 + 1) E, $F\ ^1\Sigma_g^+$–$X\ ^1\Sigma_g^+$ REMPI scheme for D_2 detection the v'_E = 0 intermediate level is the appropriate choice for detection of $X\ ^1\Sigma_g^+$ (v'' = 1 − 3) rovibrational levels, whereas the v'_E = 1 intermediate level is the better choice for detection of $X\ ^1\Sigma_g^+$ (v'' = 4, 5) rovibrational levels.

ACKNOWLEDGMENTS

This work was supported by the U.S. Department of Energy, Office of Basic Energy Sciences, Division of Chemical Sciences and in part by the U.S. National Science Foundation under NSF CHE-9322690. A.J.R.H. thanks the Netherlands Foundation for Scientific Research (Nederlandse Organisatie voor Wetenschappelijk Onderzoek) for a NWO/NATO fellowship.

REFERENCES

1. D. K. VEIRS AND G. M. ROSENBLATT, *J. Mol. Spectrosc.* **121,** 401–419 (1987).
2. A. R. W. MCKELLAR AND T. OKA, *Can. J. Phys.* **56,** 1315–1320 (1978).
3. H. BREDOHL AND G. HERZBERG, *Can. J. Phys.* **51,** 867–887 (1973).
4. C. JUNGEN, I. DABROWSKI, G. HERZBERG, AND M. VERVLOET, *J. Mol. Spectrosc.* **153,** 11–16 (1992).
5. G. H. DIEKE AND S. P. CUNNINGHAM, *J. Mol. Spectrosc.* **18,** 288–320 (1965).
6. P. SENN, P. QUADRELLI, K. DRESSLER, AND G. HERZBERG, *J. Chem. Phys.* **85,** 2384–2391 (1986).
7. P. SENN AND K. DRESSLER, *J. Chem. Phys.* **87,** 6908–6914 (1987).
8. D. J. KLIGLER AND C. K. RHODES, *Phys. Rev. Lett.* **40,** 309–313 (1978).
9. I. DABROWSKI, *Can. J. Phys.* **62,** 1639–1664 (1984).
10. G. J. GERMANN AND J. J. VALENTINI, *J. Phys. Chem.* **92,** 3792–3795 (1988).
11. E. E. MARINERO, C. T. RETTNER, AND R. N. ZARE, *Phys. Rev. Lett.* **48,** 1323–1326 (1982).
12. E. E. MARINERO, R. VASUDEV, AND R. N. ZARE, *J. Chem. Phys.* **78,** 692–699 (1983).
13. S. L. ANDERSON, G. D. KUBIAK, AND R. N. ZARE, *Chem. Phys. Lett.* **105,** 22–27 (1984).
14. J. M. GILLIGAN AND E. E. EYLER, *Phys. Rev. A.* **46,** 3676–3690 (1992).
15. N. SEN, K. RAI DASTIDAR, AND T. K. RAI DASTIDAR, *Phys. Rev. A.* **38,** 841–848 (1988).
16. K.-D. RINNEN, M. A. BUNTINE, D. A. V. KLINER, R. N. ZARE, AND W. M. HUO, *J. Chem. Phys.* **95,** 214–225 (1991).
17. R. S. FREUND, J. A. SCHIAVONE, AND H. M. CROSSWHITE, *J. Phys. Ref. Data* **14,** 235–283 (1985).
18. D. A. V. KLINER, K.-D. RINNEN, M. A. BUNTINE, D. E. ADELMAN, AND R. N. ZARE, *J. Chem. Phys.* **95,** 1663–1670 (1991).
19. J. STEADMAN AND T. BAER, *J. Chem. Phys.* **91,** 6113–6119 (1989).
20. K.-D. RINNEN, D. A. V. KLINER, M. A. BUNTINE, AND R. N. ZARE, *Chem. Phys. Lett.* **169,** 365–371 (1990).
21. R. S. BLAKE, K.-D. RINNEN, D. A. V. KLINER, AND R. N. ZARE, *Chem. Phys. Lett.* **153,** 365–370 (1988).
22. D. W. CHANDLER AND R. L. FARROW, *J. Chem. Phys.* **85,** 810–816 (1986).
23. R. L. FARROW AND D. W. CHANDLER, *J. Chem. Phys.* **89,** 1994–1998 (1988).
24. K.-D. RINNEN, D. A. V. KLINER, R. S. BLAKE, AND R. N. ZARE, *Chem. Phys. Lett.* **153,** 371–375 (1988).
25. K.-D. RINNEN, D. A. V. KLINER, R. N. ZARE, AND W. M. HUO, *Isr. J. Chem.* **29,** 369–382 (1989).
26. D. A. V. KLINER, K.-D. RINNEN, AND R. N. ZARE, *J. Chem. Phys.* **90,** 4625–4627 (1989).
27. M. A. BUNTINE, D. P. BALDWIN, R. N. ZARE, AND D. W. CHANDLER, *J. Chem. Phys.* **94,** 4672–4675 (1991).
28. M. J. J. VRAKKING, A. S. BRACKER, T. SUZUKI, AND Y. T. LEE, *Rev. Sci. Instrum.* **64,** 645–652 (1993).
29. G. D. KUBIAK, G. O. SITZ, AND R. N. ZARE, *J. Chem. Phys.* **81,** 6397–6398 (1985).
30. A. J. R. HECK, R. I. MCKAY, D. W. CHANDLER, AND R. N. ZARE, unpublished results.
31. R. L. LE ROY, *J. Chem. Phys.* **54,** 5433–5434 (1971).
32. D. M. BISHOP AND L. M. CHEUNG, *Phys. Rev. A.* **18,** 1846–1852 (1978).
33. C. SCHWARTZ AND R. J. LE ROY, *J. Mol. Spectrosc.* **121,** 420–439 (1987).
34. L. WOLNIEWICZ, *J. Chem. Phys.* **78,** 6173–6181 (1983).
35. S. YU AND K. DRESSLER, *J. Chem. Phys.* **101,** 7692–7706 (1994).
36. W. KOLOS AND J. RYCHLEWSKI, *J. Chem. Phys.* **98,** 3960–3967 (1993).
37. K. P. HUBER AND G. HERZBERG, "Constants of Diatomic Molecules," Molecular Spectra and Molecular Structure, Vol. 4. Van Nostrand-Reinhold, New York, 1979.
38. W. KOLOS AND L. WOLNIEWICZ, *J. Chem. Phys.* **50,** 3228–3240 (1969).
39. W. M. HUO AND R. L. JAFFE, *Chem. Phys. Lett.* **101,** 463–471 (1983).
40. W. M. HUO, K.-D. RINNEN, AND R. N. ZARE, *J. Chem. Phys.* **95,** 205–213 (1991).
41. P. QUADRELLI, K. DRESSLER, AND L. WOLNIEWICZ, *J. Chem. Phys.* **92,** 7461–7478 (1990).
42. T. N. KITSOPOLOUS, M. A. BUNTINE, D. P. BALDWIN, R. N. ZARE, AND D. W. CHANDLER, *Science* **260,** 1605–1610 (1993).
43. L. WOLNIEWICZ AND K. DRESSLER, *J. Chem. Phys.* **82,** 3292–3299 (1985).
44. J. W. COOLEY, *Math. Comp.* **15,** 363–374 (1961).
45. R. N. ZARE AND J. K. CASHION, University of California, Radiation Lab. Report UCRL-10881 unpublished results, 1963.
46. L. WOLNIEWICZ, submitted for publication.
47. L. WOLNIEWICZ AND K. DRESSLER, *J. Chem. Phys.* **100,** 444–451 (1994).